International Journal of Pharmaceutics 447 (2013) 94–101

Contents lists available at SciVerse ScienceDirect

International Journal of Pharmaceutics

journal homepage: www.elsevier.com/locate/ijpharm

Pharmaceutical nanotechnology

Dual anticancer drug/superparamagnetic iron oxide-loaded PLGA-based nanoparticles for cancer therapy and magnetic resonance imaging

N. Schleich[a], P. Sibret[b], P. Danhier[c], B. Ucakar[a], S. Laurent[d], R.N. Muller[d,e], C. Jérôme[b], B. Gallez[c], V. Préat[a,*,1], F. Danhier[a,1]

[a] Université Catholique de Louvain, Louvain Drug Research Institute, Pharmaceutics and Drug Delivery, Avenue Mounier, B1 73.12, 1200 Brussels, Belgium
[b] Université de Liège, Center for Education and Research on Macromolecules, Sart Tilman B6, 4000 Liège, Belgium
[c] Université Catholique de Louvain, Louvain Drug Research Institute, Laboratory of Biomedical Magnetic Resonance, Avenue Mounier, B1 73.08, 1200 Brussels, Belgium
[d] Université de Mons, Department of General, Organic, and Biomedical Chemistry, NMR and Molecular Imaging Laboratory, 7000 Mons, Belgium
[e] CMMI – Center for Microscopy and Molecular Imaging, Rue Adrienne Bolland, 8, B-6041 Gosselies, Belgium

ARTICLE INFO

Article history:
Received 3 January 2013
Received in revised form 15 February 2013
Accepted 18 February 2013
Available online 26 February 2013

Keywords:
PLGA-nanoparticles
SPIO
Paclitaxel
Cancer therapy
Magnetic resonance imaging

ABSTRACT

We developed dual paclitaxel (PTX)/superparamagnetic iron oxide (SPIO)-loaded PLGA-based nanoparticles for a theranostic purpose. Nanoparticles presented a spherical morphology and a size of 240 nm. The PTX and iron loading were 1.84 ± 0.4 and 10.4 ± 1.93 mg/100 mg respectively. Relaxometry studies and phantom MRI demonstrated their efficacy as T_2 contrast agent. Significant cellular uptake by CT26 cells of nanoparticles was shown by Prussian blue staining and fluorescent microscopy. While SPIO did not show any toxicity in CT-26 cells, PTX-loaded nanoparticles had a cytotoxic activity. PTX-loaded nanoparticle (5 mg/kg) with or without co-encapulated SPIO induced *in vivo* a regrowth delay of CT26 tumors. Together these multifunctional nanoparticles may be considered as future nanomedicine for simultaneous molecular imaging, drug delivery and real-time monitoring of therapeutic response.

1. Introduction

Theranostics is a newly emerging concept which involves simultaneous execution of therapeutic and diagnostic approaches for personalized medicine. Nanoparticles (NP) can be designed to encapsulate a wide variety of chemotherapeutic and diagnostic agents for the delivery of these agents to tumor cells (Lammers et al., 2010). Nanoparticles can target tumors by a passive process. Passive targeting implies that nanoparticles are smaller than the fenestrations of endothelial cells and can therefore enter the interstitium to be finally entrapped in the tumor. The combination of leaky vasculature and poor lymphatic drainage results in the well-known enhanced permeability and retention (EPR) effect (Maeda et al., 2000; Danhier et al., 2010).

Paclitaxel (PTX), a major anti-cancer drug has anti-neoplasic activity particularly against various types of solid tumors (Singla et al., 2002). PTX disrupts the dynamic equilibrium within the microtubule system and blocks cells in the late G_2 phase and M phase of the cell cycle, thereby inhibiting cell replication (Schiff et al., 1979). PTX is poorly soluble in water. To enhance its solubility and allow its parenteral administration, PTX is currently formulated at 6 mg/ml in a vehicle composed of a mixture of Cremophor® EL and ethanol (1:1) (Taxol®) (Weiss et al., 1990).

Magnetic resonance imaging (MRI) is a non-invasive imaging technique, presenting a high spatial resolution which is suitable for cancer detection and therapeutic response assessment (Brindle, 2008). However, its low sensitivity represents a major limitation. Superparamagnetic iron oxide (SPIO) as MRI contrast agent addresses this limitation. SPIO can produce predominant T_2 relaxation effect, resulting in a signal reduction on T_2-weighted images. The magnetic field heterogeneity around the particles, through which water molecules diffuse, induces the dephasing of the proton magnetic moments. Consequently, a T_2 effective transverse relaxation is shortened (Bjornerud and Johansson, 2004; Ling et al., 2011).

Recently, numerous publications have reported various polymer-based nanocarriers (poly(lactide-co-glycolide) (PLGA), poly (L-lactic acid) PLLA, N-(2-hydroxypropyl)methacrylamide (HPMA), poly(e-caprolactone)) for magnetic-imaging (Hamoudeh et al., 2007; Ling et al., 2011; Lu et al., 2009; Talelli et al., 2009). These theranostics successfully allowed the non-invasive assessment of the biodistribution, the visualization of drug distribution, the optimization of strategies, the prediction and real-time

* Corresponding author. Tel.: +32 2 7647320; fax: +32 2 7647398.
E-mail address: veronique.preat@uclouvain.be (V. Préat).
[1] These authors contributed the same way.

0378-5173/$ – see front matter © 2013 Elsevier B.V. All rights reserved.
http://dx.doi.org/10.1016/j.ijpharm.2013.02.042

monitoring of therapeutic responses (Lammers et al., 2010). However, these SPIO-loaded nanocarriers are generally limited because of (i) their lack of functional groups on their surface for covalent modification, (ii) their low capacity of drug loading and (iii) the fact that most of polymers used are not approved by the FDA, limiting their potential translation to the clinic.

Previously, we developed PTX-loaded PEGylated PLGA-based nanoparticles showing a lower IC_{50} *in vitro* and improved *in vivo* anti-tumor efficacy when compared to Taxol®, due to the EPR effect (Danhier et al., 2009a). (PLGA) was chosen for its biodegradability properties, its biocompatibility and its approval by the FDA (Danhier et al., 2012a). Poly(ε-caprolactone-b-ethylene glycol) (PCL-b-PEG), an amphiphilic copolymer, was added to take advantage of the repulsive properties of PEG, to provide a higher stability of nanoparticles in biological fluids and to allow the grafting of a targeting ligand (Fievez et al., 2009; Garinot et al., 2007; Pourcelle et al., 2007). We also previously developed RGD-grafted PTX-loaded PEGylated PLGA-based nanoparticles showing an effective $\alpha_v\beta_3$ targeting of the tumor endothelium (Danhier et al., 2009b).

In this study, we aimed at developing these previously described PTX-loaded PEGylated PLGA-based nanoparticles as an effective nanocarrier for dual encapsulation of anti-cancer drug (PTX) and SPIO for a theranostic purpose. Hence, SPIO were prepared by the co-precipitation technique and were encapsulated in PLGA-based nanoparticles. The physico-chemical properties of nanoparticles were characterized by different techniques such as transmission electron microscopy (TEM), dynamic light scattering (DLS) method, electron paramagnetic resonance (EPR) spectroscopy or inductively coupled plasma mass spectroscopy (ICP-MS). Their magnetic properties were evaluated using relaxometry and MRI. Furthermore, we investigated the *in vitro* cellular uptake and cytotoxicity of nanoparticles. Finally, the *in vivo* anti-tumor efficacy was assessed on CT-26 tumor-bearing mice.

2. Materials and methods

2.1. Materials

Iron(II) chloride, iron(III) chloride, oleic acid, sodium hydroxide, chlorhydric acid, 4,6-diamidino-2-phenylindole (DAPI), 3-(4,5-dimethylthiazol-2-yl)-2,5-diphenyltetrazolium bromide) (MTT), polyvinylalcohol (PVA, MW = 30–70 kDa), poly(lactic-co-glycolic acid) (PLGA, lactide/glycolide molar ratio of 50:50 MW = 7000–17 000), paclitaxel (PTX) and doxorubicin (DOX) were purchased from Sigma–Aldrich (St. Louis, MO, USA). Perls' Prussian blue kit and commercial SPIO Molday Ion™ were purchased from BioPAL (Worcester, UK). PLGA-*b*-PEG (MW = 10 040–4600), PCL-*b*-PEG (MW = 13 100–5000) and FITC-PLGA were synthesized as previously described (Danhier et al., 2009a,b; Freichels et al., 2011; Garinot et al., 2007). Dulbecco's modified Eagle's medium (DMEM), fetal bovine serum (FBS), trypsin–EDTA and penicillin–streptomycin mixtures were from Gibco® BRL (Carlsbad, CA, USA). Murine colon carcinoma CT26 cells were kindly given by Goldyne Savad Institute of Gene Therapy, Hadassah-Hebrew University Hospital (Jerusalem, Israël). Water used in all experiment was prepared by Aqualab purification system.

2.2. Synthesis of superparamagnetic iron oxides (SPIO) coated with oleic acid

Hydrophobic superparamagnetic iron oxides (SPIO) were synthesized using a classical co-precipitation technique of ferrous and ferric salts in alkaline medium (Massart, 1981). Briefly, 10 mmol iron(III) chloride and 5 mmol iron(II) chloride were mixed together in 12 ml of an hydrochloride aqueous solution (HCl 1 M). This solution was then added dropwise to an aqueous solution of NaOH 1 M containing 3.1 g of oleic acid with stirring on a magnetic stir plate for 20 min under a nitrogen-gas atmosphere at 80 °C. The black precipitate was separated using a magnet, washed three times using absolute ethanol and then dissolved in 50 ml of dichloromethane (DCM). The solution was then placed in an ultrasonic bath for 10 min and centrifuged (4416 rcf, 10 min) to remove the undispersed residue.

Hydrophilic SPIO used as SPIO aqueous solution (SPIO sol) were also synthesized. Briefly 1 ml of DCM dispersion of SPIO coated with oleic acid (40 mg/ml) was added to a suspension of tetramethylammonium 11-aminoundecanoate in DCM (40 mg in 2 ml). After 24 h magnetic stirring, the precipitate was washed three times with DCM and dispersed in water (Yang et al., 2010).

2.3. Preparation of PLGA-based nanoparticles loaded with SPIO and paclitaxel or doxorubicin

Both nanoparticles loaded with SPIO and DOX (SPIO/DOX-NP) and nanoparticles loaded with SPIO and paclitaxel (SPIO/PTX-NP) were prepared by an emulsion–diffusion–evaporation method (Danhier et al., 2009a; Garinot et al., 2007) Briefly, PLGA (14 mg/ml), PLGA-PEG (3 mg/ml) and PCL-PEG (3 mg/ml) were dissolved in 2 ml DCM containing SPIO (Fe concentration: 15 mg/ml). Doxorubicin HCl (0.2 mg/ml) was dissolved in 1 ml DCM containing 0.001 mg/ml triethanolamine beforehand and stirred overnight (Shieh et al., 2011) whereas paclitaxel (3 mg) was added directly. This organic solution was then added to an aqueous solution (4.5 ml) containing 3% (p/v) PVA and emulsified using a vortex for 2 min followed by sonication (2× 30 s, 50 W). The mixture was then added dropwise and under magnetic stirring into an aqueous solution containing 1% PVA and stirred overnight to evaporate the organic solvent. To remove the non-encapsulated drug, the suspension was filtered (1.2 μm) and washed three times with water using ultracentrifugation (11,000 × *g*, 30 min, 4 °C) and suspended in 2 ml water. FITC covalently labeled PLGA was used to prepare fluorescent nanoparticles (Freichels et al., 2011). PTX-loaded nanoparticles (PTX-NP) and SPIO-loaded nanoparticles (SPIO-NP) were also prepared using the same protocol.

2.4. Physico-chemical characterization of nanoparticles loaded with SPIO and paclitaxel or doxorubicin

2.4.1. Thermogravimetric analysis of SPIO

The coating percentage of SPIO with oleic acid was assessed by thermogravimetric analysis (TGA) on a TA Instrument Q500 model, under dry nitrogen flow, with a heating rate of 15 °C/min from RT to 600 °C, in an open platinum pan.

2.4.2. Particles size and morphology determination

The hydrodynamic particle size and size polydispersity of nanoparticles was assessed using a dynamic light scattering method (Nano ZS, Malvern instruments, UK). The Zeta (ζ) potential of the nanoparticles was measured in KCL 1 mM with a Malvern Nano ZS at 25 °C. The morphology of the particles was achieved using transmission electron microscopy (TEM). TEM was carried out with a Philips CM 100 operating at a voltage of 100 kV, equipped with a Megaview G2 camera. Samples for TEM experiments were prepared by spin coating a drop of nanoparticles in DCM on a carbon-coated TEM grid.

2.4.3. Determination of SPIO loading content

The iron content was measured by electron paramagnetic resonance (EPR) using a Bruker EMX EPR spectrometer operating at 9 GHz (Bruker Biospin GmBh, Germany) validated by inductively

coupled plasma mass spectroscopy (ICP-MS) measurements (Agilent 7500ce instrument) (Danhier et al., 2012b). Typical parameters were selected for EPR measurements: 3 mT modulation amplitude, 10.11 mW power, 325.1 mT center field, and field 400 mT sweep width. Double integration of the iron oxides EPR spectra was used to quantify signal intensity.

2.4.4. Determination of drug loading content

The DOX content was assessed by determining the absorbance at 480 nm with a UV–visible spectrophotometer (HP8453 from Hewlett Packard). The PTX content was determined using high-performance liquid chromatography (HPLC) with UV detection at 227 nm (Agilent 1100 series, Agilent Technologies, Diegem, BE), as previously described after dissolution of particles in acetonitrile (50:50), vortex (5 min) and filtration (0.22 μm) (Danhier et al., 2009b). The mobile phase consisted of acetonitrile and water (70:30 v/v, respectively) at a rate of 1 ml/min. The column used was a CC 125/4 Nucleod UR 100-5 C18. Standard solutions of 5–100 μg/ml of PTX dissolved in acetonitrile were used for calibration (correlation coefficient = 0.99, LOD = 1.6 μg/ml, LOQ = 5 μg/ml, coefficients of variation < 4.5%). The drug loading was defined as the amount of drug (mg) loaded for 100 mg of polymer whereas the encapsulation efficiency was defined by the ratio of the encapsulated drug compared to the initial amount of drug (Danhier et al., 2010).

2.5. Magnetic properties

2.5.1. Relaxometry by proton NMRD

Nuclear Magnetic Relaxation Dispersion (NMRD) profiles were recorded at 37 °C on a Fast Field Cycling Relaxometer (Stelar, Mede, Italy) over a magnetic field range from 0.01 to 40 MHz. Additional longitudinal (R_1) and transverse (R_2) relaxation rate measurements at 20 and 60 MHz were respectively obtained on Minispec mq 20 and mq 60 spin analyzers (Bruker, Karlsruhe, Germany). The fitting of the NMRD profiles by a theoretical relaxation model allows the determination of the crystal radius (r) and the specific magnetization (M_S). The proton NMRD curves were fitted using data-processing software, including different theorical models describing the nuclear relaxation phenomena (Laurent et al., 2010; Roch et al., 1999, 2005).

2.5.2. Phantom MRI

T_2 relaxivity was obtained using a 11.7 T animal Biospec MR system (Bruker Biospec, Ettlingen, Germany). Phantom MRI of SPIO-NP was carried out at various iron concentration from 0 μg/ml to 30 μg/ml (0, 5, 10, 15, 20, 25 and 30 μg/ml) in 10% gelatin using a T_2-weighted multi-slice multi-echo (MSME) sequence. The imaging parameters were: repetition time (TR) = 2500 ms, echo time (TE) = 30 ms, field of view (FOV) = 3.00 cm, flip angle (FA) = 180.0°.

2.6. In vitro cell line experiment

2.6.1. In vitro cellular uptake

CT26 colon carcinoma cells were seeded at a density of 1×10^5 cells per well in Lab-tekII® chamber slide system in DMEM supplemented with 10% fetal bovine serum (FBS), 1% of a penicillin/streptomycin mixture and 1% L-Glutamine. Cells were incubated for 24 h in a 5% CO_2 incubator (37 °C). Then, 100 μl of SPIO/DOX-NP suspension labeled with FITC was added to the medium for 1 h, 2 h or 4 h. After incubation, cells were fixed at room temperature for 15 min with 4% paraformaldehyde. Following cell fixation, cells were incubated with 4,6-diamidino-2-phenylindole (DAPI) at a concentration of 0.2 μg/ml in phosphate buffer saline (PBS) for 15 min protected from light, washed twice with PBS and once with water to avoid salt crystals formation.

The intracellular iron oxides were visualized using a Prussian blue staining. After 2 h of incubation with SPIO/DOX-NP suspension at 80 μg/ml of Fe concentration, CT-26 were washed three times with PBS, fixed with 4% paraformaldehyde for 15 min and incubated for 30 min with 2 ml working solution provided by the Prussian blue kit comprising equal volume of 2% HCl and 2% potassium ferrocyanide (II) trihydrate (bioPAL). Wells were finally washed twice with PBS and once with water.

The stained plates were observed using either a fluorescent microscope (Axioskop 40, Zeiss) fitted with three excitation filters: 340/380 nm (blue), 470/490 nm (green), 515/560 nm (red) or without filter for iron oxide visualization. Photographs were taken with an AxioCam MRc5 camera (Zeiss).

2.6.2. In vitro cytotoxicity

The cytotoxicity of SPIO, SPIO-NP and SPIO/PTX-NP was determined by a MTT cell proliferation assay as previously described (Danhier et al., 2009a,b; Mosmann, 1983). Briefly, CT26 colon carcinoma cells were seeded at a density of 10^4 cell per well in 96-well plates. Next day, cells were incubated with the different formulations: SPIO solution, SPIO-NP, PTX-NP at 3 different PTX concentrations (20 μg/ml, 10 μg/ml and 2 μg/ml) and SPIO/PTX-NP. All the concentrations of SPIO used were based on the corresponding PTX aforementioned concentrations when SPIO and PTX are co-loaded (Fe concentrations: 106.8 μg/ml, 53.4 μg/ml and 10.7 μg/ml). After 24 h, supernatants were removed. Wells were then washed twice with PBS and incubated with DMEM containing MTT (5 mg/ml) for an additional 2 h. After MTT solution removal, DMSO was added to dissolve the formazan crystals. Absorbance was measured at 570 nm using a BioRad microplate reader. Untreated cells were taken as control with 100% viability, and Triton X-100 1% was used as a positive control of cytotoxicity. Cells without addition of MTT were used as blank to calibrate the spectrophotometer to zero absorbance.

2.7. In vivo evaluation

2.7.1. Animal and tumor models

All experiments were performed in compliance with guidelines set by national regulations and were approved by the ethical committee for animal care of the health science sector of the Université Catholique de Louvain. CT26 colon carcinoma cells were inoculated subcutaneously in the right flank of BALB/c mice (5×10^4 cells per mouse).

2.7.2. In vivo anti-tumor efficacy

The effect of SPIO/PTX-NP on tumor growth was assessed by daily measurements of tumor volume with an electronic caliper. CT26 cells were injected subcutaneously in the right flank of the mice to allow easy and reproducible tumor volume measurements. Mice were randomly assigned to a treatment group when tumor reached a volume of $27 \pm 5\ mm^3$. Treatment was injected trough the tail vein. Five groups were defined (6 mice per group): group1: PBS injection, group 2: injection of a SPIO solution (SPIO sol; Fe dose: 13.5 mg/kg), group 3: injection of SPIO loaded nanoparticles (SPIO-NP; Fe dose: 13.5 mg/kg), group 4: injection of PTX loaded nanoparticles (PTX-NP) at a dose of 5 mg/kg PTX and group 5: injection of SPIO-PTX co-loaded nanoparticles (SPIO/PTX-NP; PTX dose: 5 mg/kg – Fe dose: 13.5 mg/kg). The end point of the experiment was determined as the moment when tumor reached 600 mm^3. At this point, mice were sacrificed. Tumor growing ratio was calculated as the volume measured each day (mm^3) compared to the volume measured at day 1 (day of treatment injection).

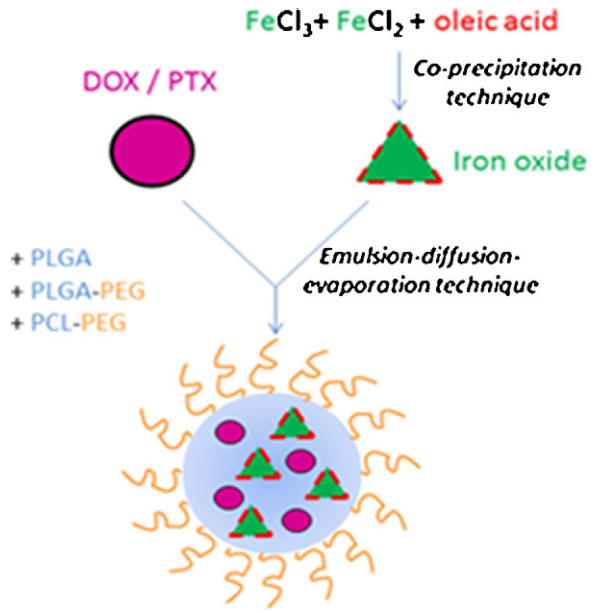

Fig. 1. Schematic representation of SPIO/PTX-loaded PLGA-based nanoparticles.

2.8. Statistical analyses

All results are expressed as mean ± standard deviation (SD). Two-way ANOVA, Bonferroni post test, Kaplan–Meier survival rate and *T*-test were performed, using the software GraphPad Prism 5 for Windows, to demonstrate statistical differences ($p < 0.05$).

3. Results and discussion

3.1. Physico-chemical characterization

To ensure dispersibility in organic solvent and hydrophobicity of particles, SPIO were coated with oleic acid by a simple adsorption process (Fig. 1). Coating efficacy was assessed by the percent by mass of inorganic matters using TGA. SPIO showed a percentage of 39.5% inorganic matters representing SPIO suggesting a coating of 60.5%. This coating is needed to prevent the formation of large aggregates when exposed to the biological system or DCM for nanoparticle preparation (van Ewijk et al., 1999).

SPIO were also characterized in terms of size and morphology using transmission electron microscopy (TEM) (Fig. 2A). TEM results showed a spherical morphology with relatively uniform sizes ranging from 6 to 12 nm. Apparent aggregation was not detected.

PLGA-based nanoparticles were prepared using an emulsion–diffusion–evaporation method (Garinot et al., 2007) (Fig. 1). This method was selected comparing the results obtained either by the nanoprecipitation or by the emulsion method after several adjusts (data not shown). As shown in Table 1, all the PLGA-based nanoparticles presented neutral ζ potentials and similar sizes between 235 nm and 244 nm ($p > 0.05$) except for the PLGA-based nanoparticles loaded with both SPIO and doxorubicin (SPIO/DOX-NP), which presented a slightly larger size (285 nm). It is well known that the EPR effect is exploited to allow nanocarriers the passive targeting of tumors. Thus, the particle size plays an important role. Endothelial pores have sizes varying from 10 to 1000 nm. It was further established that the optimal particles size is ranging from 20 to 400 nm (Danhier et al., 2010; Maeda et al., 2000). PTX/SPIO-loaded nanoparticles are thus convenient to benefit from the EPR effect.

The size and morphology of SPIO-PTX-loaded nanoparticles were also investigated by TEM. Particles were spherical and presented a narrow distribution without aggregation. Particles size appeared to be approximately 50 nm. Only iron oxides induced differences in transmission and consequently in contrast. The measured size does not probably constitute the real size of nanoparticles, in comparison with the hydrodynamic diameter measured by DLS. The polymers shape was visible in gray areas surrounding black spots (SPIO). Interestingly, size, morphology or distribution of nanoparticles were not affected by the co-encapsulation of SPIO and PTX (Fig. 2B and C).

All formulations presented a similar iron loading around 10 mg/100 mg of polymer ($p > 0.05$) which is similar to those found in the literature (Guthi et al., 2010; Hu et al., 2012; Lee et al., 2010) The Fe concentration was the same when quantified by EPR spectroscopy or by ICP-MS.

PTX encapsulation efficiency (24.2 ± 5.7% and 24.8 ± 4.9% for PTX-NP and SPIO/PTX-NP, respectively ($p > 0.05$)) and drug loading were not affected by the co-encapsulation of SPIO. The PTX loading was 1.8 mg/100 mg polymer. Drug loading is crucial for formulations of drug delivery systems because it directly affects the therapeutic dose available for the targeted tissue. Interestingly, the drug loading of nanoparticles, formulated by an emulsion–diffusion–evaporation method using PVA as emulsifier, was 4.5-fold higher than with the same method, described previously, using sodium cholate and 2.5-fold higher than with the nanoprecipitation technique (Danhier et al., 2009a). Moreover, the drug loading of nanoparticles was 2.8–4.8-fold higher than those described in previous studies (Hu et al., 2012; Singh et al., 2011). Due to the small amount of doxorubicin used to formulate SPIO/DOX-NP (0.5 mg/100 mg of polymer), the encapsulation efficiency reached 100%.

3.2. Magnetic properties of SPIO and SPIO-NP

3.2.1. Relaxometry studies

The relaxivity of SPIO is defined as the efficiency to enhance the relaxation rate of the neighboring water protons and is expressed in $s^{-1}\,mM^{-1}$. The relaxivities of SPIO are summarized in Table 2. Noticeably, the r_2/r_1 ratios of SPIO are higher than those of Resovist® (Allkemper et al., 2002), indicating that SPIO could be considered as highly efficient T_2 contrast agents.

The NMRD profiles which display the evolution of proton longitudinal relaxivity as a function of the applied field, illustrates typically superparamagnetic relaxation profiles both for SPIO-loaded nanoparticles and SPIO/PTX-loaded nanoparticles (Fig. 3). The shape of the NMRD profile of superparamagnetic iron oxide

Table 1
Particle size, ζ potential, drug encapsulation efficiency, drug loading and SPIO loading of PLGA-based nanoparticles loaded with either SPIO (SPIO-NP), paclitaxel (PTX-NP), SPIO and paclitaxel (SPIO/PTX-NP) or with SPIO and doxorubicin (SPIO/DOX-NP) ($n = 3$).

	SPIO-NP	PTX-NP	SPIO/PTX-NP	SPIO/DOX-NP
Size (nm)	235.8 ± 8.9	238.5 ± 8.8	243.8 ± 9.9	285.0 ± 1.25
ζ potential (mV)	−0.16 ± 0.04	−0.05 ± 0.01	−0.02 ± 0.01	−2.42 ± 0.56
Drug encapsulation efficiency (%)	–	24.2 ± 5.7	24.8 ± 4.9	100 ± 0.0
Drug loading (mg/100 mg polymer)	–	1.83 ± 0.3	1.84 ± 0.4	0.5 ± 0.0
Iron loading (mg/100 mg polymer)	9.0 ± 1.53	–	10.4 ± 1.93	8.6 ± 0.63

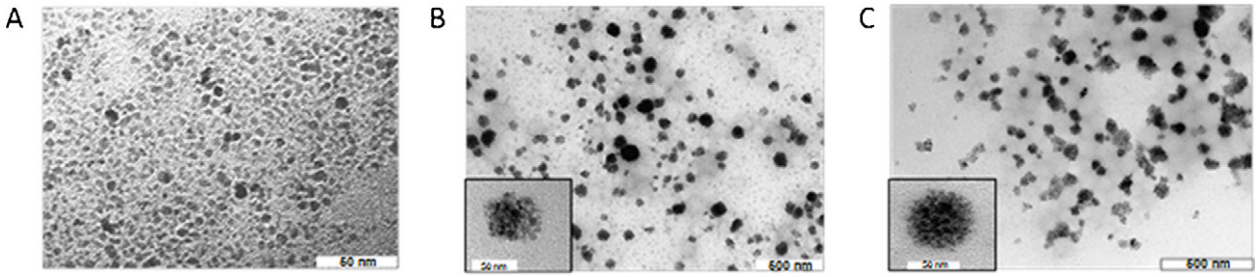

Fig. 2. TEM micrographs of (A) SPIO, (B) SPIO-NP and (C) SPIO/PTX-NP.

Table 2
Longitudinal (r_1) and transverse (r_2) relaxivities of SPIO-NP, SPIO/PTX-NP and Resovist® at 20 and 60 MHz in water (37 °C).

	20 MHz			60 MHz		
	r_1 (mM^{-1} s^{-1})	r_2 (mM^{-1} s^{-1})	r_2/r_1 (mM^{-1} s^{-1})	r_1 (mM^{-1} s^{-1})	r_2 (mM^{-1} s^{-1})	r_2/r_1 (mM^{-1} s^{-1})
SPIO-NP	3.4	134.4	39.5	1.1	139	126.4
SPIO/PTX-NP	3.8	127	33.4	1.3	137	105.4
Resovist®(Allkemper et al., 2002)	25	119	4.8	NA	NA	NA

NA, not available.

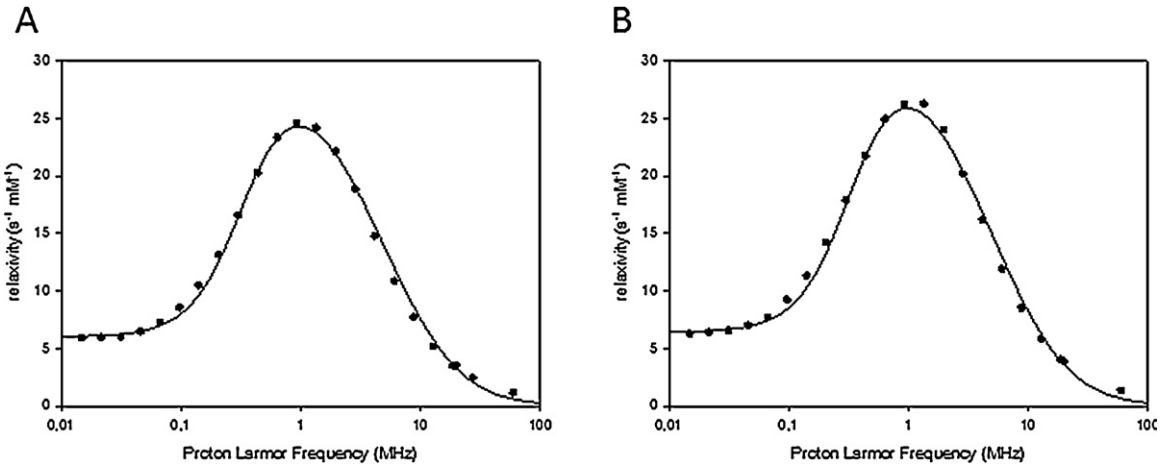

Fig. 3. ^{1}H NMRD relaxivity profiles of (A) SPIO-loaded nanoparticles and (B) SPIO/PTX-loaded nanoparticles.

nanoparticle suspensions is governed (i) by the size, the crystallinity and the magnetization of the magnetic cores, (ii) by the diffusion of solvent close to the particle cores, and (iii) by the interaction between superparamagnetic cores, as they affect the anisotropy energy (Roch et al., 1999). Table 3 shows the parameters obtained from the theoretical fitting of the NMRD profiles. The specific magnetization (M_S), the crystal radius (r) and the Néel relaxation time (τ_N) highlight the superparamagnetism properties of SPIO. Interestingly, the presence of PTX into nanoparticles did not change significantly the relaxometric properties.

3.2.2. Phantom MRI

Various concentrations of SPIO in aqueous solution (SPIO sol) and PLGA-based nanoparticles loaded with SPIO (SPIO-NP) ranging from 0 to 30 μg/ml (Fe concentrations: 0-5-10-15-20-25-30 μg/ml) were investigated by T_2-weighted MRI to assess their T_2 enhancing capability. Commercial SPIO (BioPAL, Worcester, UK) were used as a reference at the same concentrations (Fig. 4). This pilot experiment confirmed that the magnetism of the synthesized SPIO was detectable by MRI either when freely suspended in water (SPIO sol) or when encapsulated in PLGA-based nanoparticles (SPIO-NP). For all treatments, the signal intensity of MRI decreased as the SPIO concentration increased. It is important to note that synthesized SPIO presented similar relaxation rates ($R_2 = T_2^{-1}$) profiles than commercialized SPIO (BioPAL). Furthermore, as shown on Fig. 4A, the transverse relaxation rates (T_2^{-1}) of all treatments were well fitted by a line within the analyzed range of iron concentration. Nevertheless, compared to SPIO sol, SPIO-NP relaxed more slowly indicating that the presence of PLGA surrounding SPIO could slightly affect T_2 enhancing capability.

Table 3
Parameters obtained from the theoretical fitting of the NMRD profiles.

	SPIO-NP	SPIO/PTX-NP
M_S (Am^2/kg)	14.5 ± 0.1	15.1 ± 0.1
r (nm)	16.1 ± 0.1	15.9 ± 0.1
τ_N (ns)	5.88 ± 0.08	5.78 ± 0.08

3.3. In vitro cellular uptake

To assess the uptake of SPIO/DOX-NP, fluorescent NP were used. Fluorescein isothiocyanate (FITC) was grafted covalently on PLGA to label polymer matrix (green fluorescence). Doxorubicin was chosen because of its natural fluorescence (red fluorescence) to follow the drug into cells. Nuclei of cells were labeled using DAPI staining (blue fluorescence). Fig. 5A shows that DOX fluorescence increased

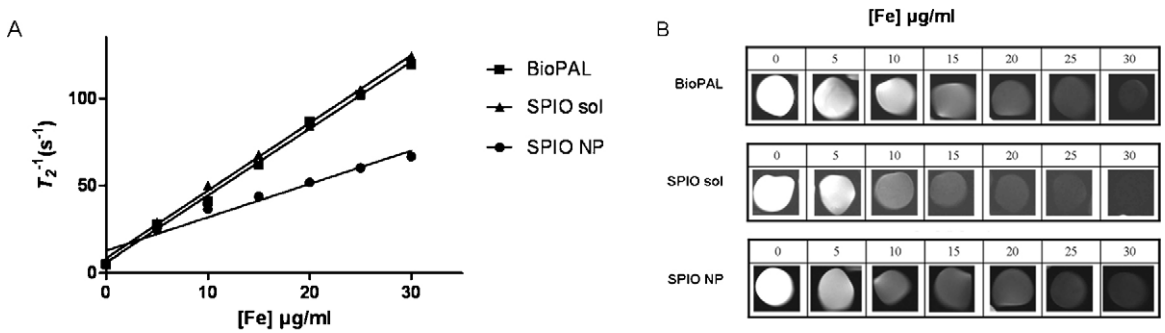

Fig. 4. (A) T_2 relaxation rate of commercial SPIO (BioPAL, Worcester, UK), an aqueous suspension hydrophilic SPIO (SPIO sol) and SPIO loaded nanoparticles (SPIO NP) as a function of Fe concentration (μg/ml). (B) T_2-weighted MR images as a function of Fe concentration (μg/ml, TE = 30 ms).

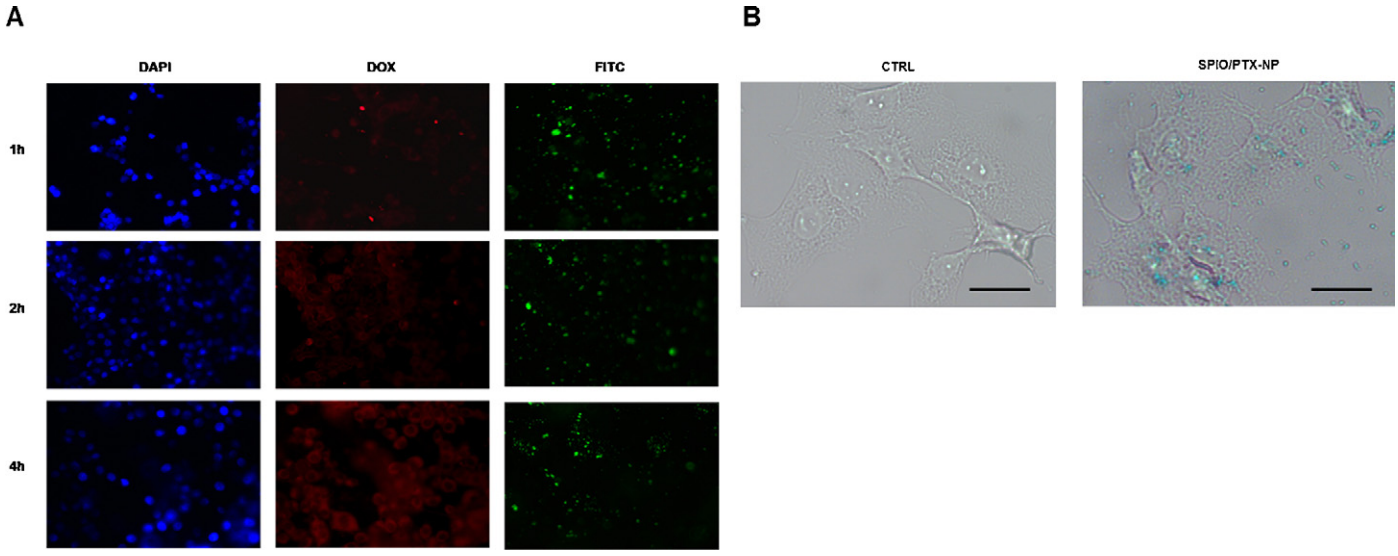

Fig. 5. Nanoparticles uptake by CT26 cells. (A) Fluorescence microscopy of CT26 cells (1×10^5) after 1, 2 or 4 h of incubation with SPIO/DOX-NP followed by DAPI staining (magnification = 40×). (B) Prussian blue staining images after 4 h of incubation with SPIO/PTX-NP at a Fe concentration of 80 μg/ml, treated with prussian blue liquid for 30 min. Black lines correspond to 10 μm.

with the incubation time of the formulation. Moreover, the red and blue fluorescence were co-localized indicating that DOX was able to reach the nucleus which is its site of action. FITC-fluorescence indicated that polymeric nanoparticles have also been internalized by cells allowing a broad distribution of free DOX and SPIO in the cytosol. After 4 h, the blue fluorescence (DAPI) was co-localized with DOX, indicating that DOX accumulated in nuclei. The cellular uptake was thus time-dependent, as reported previously (Danhier et al., 2009a).

Fig. 5B shows the entrapment of SPIO stained in intense blue color into the cells. Obviously, there was no blue color appearance in cells of the control group. Conversely, cells incubated with SPIO/PTX-NP (Fe concentration = 80 μg/ml) were stained in intensive blue color. Consistent with previous publications, blue areas or spots could be seen in almost every cell (Ling et al., 2012). SPIO-loaded PLGA nanoparticles were internalized by cells PLGA nanoparticles are mostly internalized through fluid phase pinocytosis and also through clathrin-mediated endocytosis (Petros and Desimone, 2010; Danhier et al., 2012a).

3.4. In vitro cytotoxicity

The cytotoxicity of multifunctional nanoparticles was evaluated by the MTT test in CT26 colon carcinoma cells after 24 h incubation (Fig. 6). The range of PTX concentrations (2–20 μg/ml) corresponds to plasma levels of the drug achievable in human (Raymond et al.,

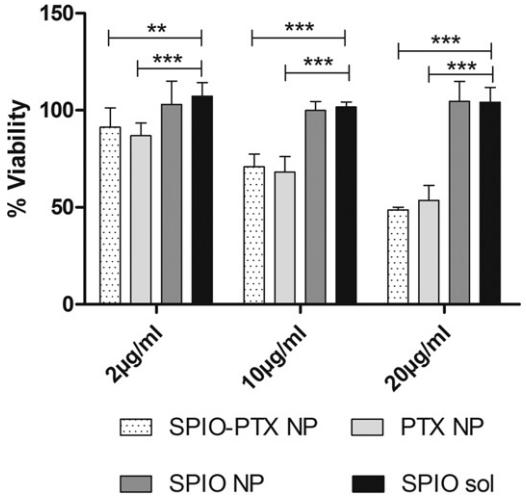

Fig. 6. Viability of CT26 cells incubated with a solution of hydrophilic SPIO (SPIO sol, SPIO concentration corresponding to SPIO/PTX-NP formulation: Fe concentration of 106.8 μg/ml, 53.4 μg/ml and 10.7 μg/ml), paclitaxel-free nanoparticles (SPIO-NP, same concentrations as above), nanoparticles loaded with paclitaxel (PTX-NP, PTX concentrations 2, 10 and 20 μg/ml) and nanoparticles loaded with paclitaxel and SPIO (SPIO/PTX-NP). Cell viability was determined by the MTT assay. Untreated cells were taken as a negative control and Triton X-100 1% was used as a positive control. The results were expressed as mean values ± standard deviation ($n = 5$). $^{**}p < 0.01$, $^{***}p < 0.001$.

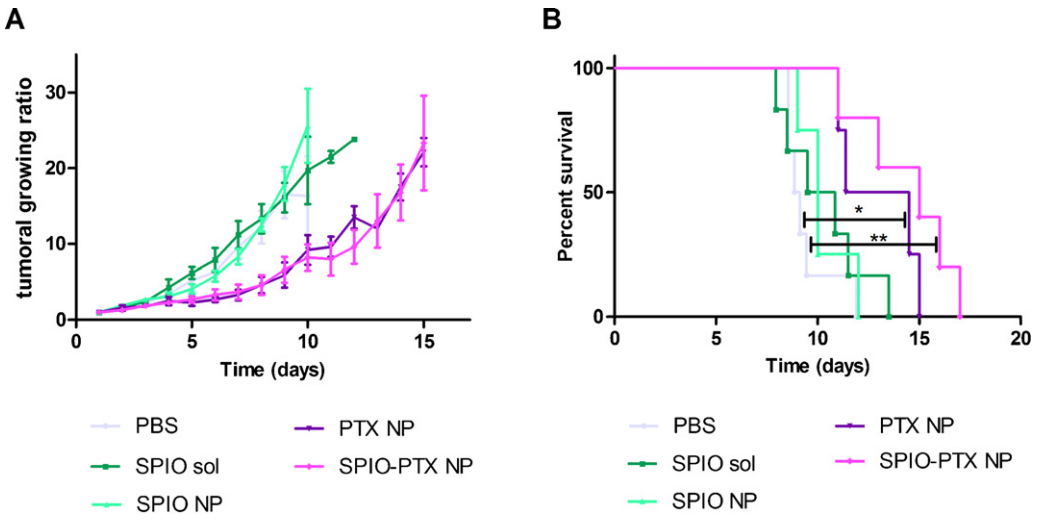

Fig. 7. (A) Tumor growth curves of CT26-tumor bearing mice treated with free SPIO in aqueous solution (SPIO sol), SPIO loaded nanoparticles (SPIO-NP), paclitaxel-loaded nanoparticles (PTX-NP) (PTX dose = 5 mg/kg), paclitaxel and SPIO co-loaded nanoparticles (SPIO/PTX-NP) (PTX dose = 5 mg/kg) or untreated (PBS). The treatment was injected in the tail vein of the mice when tumors reached 27 ± 5 mm (n = 6/group). Results are presented as the average tumor growing ratio ± SEM versus time after treatment injection. (B) Survival rates of tumor-bearing mice.

1997). The range of Fe concentrations (106.8 μg/ml, 53.4 μg/ml and 10.7 μg/ml) corresponds to the concentrations present in solution of the different tested concentrations of PTX. An aqueous solution containing hydrophilic SPIO was used to test the toxicity of free SPIO (without entrapment into nanoparticles; SPIO sol). Consistent with other published data (Ling et al., 2011, 2012), SPIO (in solution or entrapped into NP) did not present any cytotoxic activity. The addition of PTX in formulations induced cell death. Compared with SPIO or SPIO-NP, the viability of cells treated with PTX-NP and SPIO/PTX-NP was decreased ($p < 0.01$). This PTX cytotoxicity was increased in dose-dependent manner. Hence, PTX anti-tumor efficacy was maintained while encapsulated in PLGA-based nanoparticles in presence or in absence of SPIO.

3.5. *In vivo* anti-tumor efficacy

The *in vivo* anti-tumor efficacy of multifunctional nanoparticles was evaluated in CT26-tumor-bearing mice (Fig. 7). Consistent with *in vitro* cytotoxicity data, all treatments containing PTX (PTX-NP and SPIO/PTX-NP) induced a higher delay in tumor growth than other treatments (Fig. 7A). Moreover, SPIO sol and SPIO-NP did not inhibit the tumor growth when compared with the PBS control group (Fig. 7A). Interestingly, we also demonstrated in a previous study that PTX-NP treated mice presented a higher delay in tumor growth compared to the group treated with free PTX (Danhier et al., 2009a). Kaplan–Meier survival rate was performed (Fig. 7B). PTX-NP and SPIO/PTX-NP exhibited higher survival rates than the untreated group (PBS) with median survival rates of 13 and 15 days, respectively, compared to 9 days ($p < 0.05$ and $p < 0.01$). No significant difference was observed between the two PTX-based treatment ($p > 0.05$). Additionally, SPIO sol and SPIO-NP presented median survival times of 10.2 and 10 days ($p > 0.05$), which are not statistically different than the control PBS group ($p > 0.05$).

4. Conclusions

Based on previously developed PLGA-based nanoparticles for anti-tumor drugs delivery, we aimed to extent these nanoparticles as multifunctional entities by co-encapsulation of an anti-cancer drug (PTX) and contract agents (SPIO) for both anti-cancer therapy and magnetic resonance imaging. We successfully co-encapsulated SPIO and PTX in PLGA-based nanoparticles. We demonstrated that these nanoparticles inhibited the growth of CT26 cells. PTX/SPIO-loaded nanoparticles could be used as potential tumor-targeting MRI contrast agents, thanks to the high uptake of nanoparticles by cells as well as their magnetic characteristics. Together these results, these multifunctional nanoparticles may be considered as future nanomedicine for simultaneous targeting imaging, drug delivery and real-time monitoring of therapeutic response. In the future, these multifunctional nanoparticles will be grafted with a RGD peptide to be used as tumor targeted theranostic nanoparticles. RGD-grafted PLGA nanoparticles have been shown to target the $\alpha_v\beta_3$ integrin of the tumor endothelium and prolong survival time of mice when compared to non-targeted nanoparticles (Danhier et al., 2009b).

References

Allkemper, T., Bremer, C., Matuszewski, L., Ebert, W., Reimer, P., 2002. Contrast-enhanced blood-pool MR angiography with optimized iron oxides: effect of size and dose on vascular contrast enhancement in rabbits. Radiology 223, 432–438.
Bjornerud, A., Johansson, L., 2004. The utility of superparamagnetic contrast agents in MRI: theoretical consideration and applications in the cardiovascular system. NMR Biomed. 17, 465–477.
Brindle, K., 2008. New approaches for imaging tumour responses to treatment. Nat. Rev. Cancer 8, 94–107.
Danhier, F., Lecouturier, N., Vroman, B., Jérôme, C., Marchand-Brynaert, J., Feron, O., Préat, V., 2009a. Paclitaxel-loaded PEGylated PLGA-based nanoparticles: in vitro and in vivo evaluation. J. Control. Release 133, 11–17.
Danhier, F., Vroman, B., Lecouturier, N., Crokart, N., Pourcelle, V., Freichels, H., Jérôme, C., Marchand-Brynaert, J., Feron, O., Préat, V., 2009b. Targeting of tumor endothelium by RGD-grafted PLGA-nanoparticles loaded with paclitaxel. J. Control. Release 140, 166–173.
Danhier, F., Feron, O., Préat, V., 2010. To exploit the tumor microenvironment: passive and active tumor targeting of nanocarriers for anti-cancer drug delivery. J. Control. Release 148, 135–146.
Danhier, F., Ansorena, E., Silva, J.M., Coco, R., Le Breton, A., Préat, V., 2012a. PLGA-based nanoparticles: an overview of biomedical applications. J. Control. Release 161, 505–522.
Danhier, P., De Preter, G., Boutry, S., Mahieu, I., Leveque, P., Magat, J., Haufroid, V., Sonveaux, P., Bouzin, C., Feron, O., Muller, R.N., Jordan, B.F., Gallez, B., 2012b. Electron paramagnetic resonance as a sensitive tool to assess the iron oxide content in cells for MRI cell labeling studies. Contrast Media Mol. Imaging 7, 302–307.
Fievez, V., Plapied, L., des, R.A., Pourcelle, V., Freichels, H., Wascotte, V., Vanderhaeghen, M.L., Jérôme, C., Vanderplasschen, A., Marchand-Brynaert, J., Schneider, Y.J., Préat, V., 2009. Targeting nanoparticles to M cells with non-peptidic ligands for oral vaccination. Eur. J. Pharm. Biopharm. 73, 16–24.
Freichels, H., Danhier, F., Préat, V., Lecomte, P., Jérôme, C., 2011. Fluorescent labeling of degradable poly(lactide-co-glycolide) for cellular nanoparticles tracking in living cells. Int. J. Artif. Organs 34, 152–160.

Garinot, M., Fievez, V., Pourcelle, V., Stoffelbach, F., des Rieux, A., Plapied, L., Theate, I., Freichels, H., Jérôme, C., Marchand-Brynaert, J., Schneider, Y.J., Préat, V., 2007. PEGylated PLGA-based nanoparticles targeting M cells for oral vaccination. J. Control. Release 120, 195–204.

Guthi, J.S., Yang, S.G., Huang, G., Li, S., Khemtong, C., Kessinger, C.W., Peyton, M., Minna, J.D., Brown, K.C., Gao, J., 2010. MRI-visible micellar nanomedicine for targeted drug delivery to lung cancer cells. Mol. Pharmacol. 7, 32–40.

Hamoudeh, M., Al, F.A., Canet-Soulas, E., Bessueille, F., Leonard, D., Fessi, H., 2007. Elaboration of PLLA-based superparamagnetic nanoparticles: characterization magnetic behaviour study and in vitro relaxivity evaluation. Int. J. Pharm. 338, 248–257.

Hu, J., Qian, Y., Wang, X., Liu, T., Liu, S., 2012. Drug-loaded and superparamagnetic iron oxide nanoparticle surface-embedded amphiphilic block copolymer micelles for integrated chemotherapeutic drug delivery and MR imaging. Langmuir 28, 2073–2082.

Lammers, T., Kiessling, F., Hennink, W.E., Storm, G., 2010. Nanotheranostics and image-guided drug delivery: current concepts and future directions. Mol. Pharmacol. 7, 1899–1912.

Laurent, S., Bridot, J.L., Elst, L.V., Muller, R.N., 2010. Magnetic iron oxide nanoparticles for biomedical applications. Future. Med Chem. 2, 427–449.

Lee, P.W., Hsu, S.H., Wang, J.J., Tsai, J.S., Lin, K.J., Wey, S.P., Chen, F.R., Lai, C.H., Yen, T.C., Sung, H.W., 2010. The characteristics biodistribution, magnetic resonance imaging and biodegradability of superparamagnetic core-shell nanoparticles. Biomaterials 31, 1316–1324.

Ling, Y., Wei, K., Luo, Y., Gao, X., Zhong, S., 2011. Dual docetaxel/superparamagnetic iron oxide loaded nanoparticles for both targeting magnetic resonance imaging and cancer therapy. Biomaterials 32, 7139–7150.

Ling, Y., Wei, K., Zou, F., Zhong, S., 2012. Temozolomide loaded PLGA-based superparamagnetic nanoparticles for magnetic resonance imaging and treatment of malignant glioma. Int. J. Pharm. 430, 266–275.

Lu, J., Ma, S., Sun, J., Xia, C., Liu, C., Wang, Z., Zhao, X., Gao, F., Gong, Q., Song, B., Shuai, X., Ai, H., Gu, Z., 2009. Manganese ferrite nanoparticle micellar nanocomposites as MRI contrast agent for liver imaging. Biomaterials 30, 2919–2928.

Maeda, H., Wu, J., Sawa, T., Matsumura, Y., Hori, K., 2000. Tumor vascular permeability and the EPR effect in macromolecular therapeutics: a review. J. Control. Release 65, 271–284.

Massart, R., 1981. Preparation of aqueous magnetic liquids in alkaline and acidic media. IEEE Transactions on Magnetics 17, 1247–1248.

Mosmann, T., 1983. Rapid colorimetric assay for cellular growth and survival: application to proliferation and cytotoxicity assays. J. Immunol. Methods 65, 55–63.

Petros, R.A., Desimone, J.M., 2010. Strategies in the design of nanoparticles for therapeutic applications. Nat. Rev. Drug Discov. 9, 615–627.

Pourcelle, V., Devouge, S., Garinot, M., Preat, V., Marchand-Brynaert, J., 2007. PCL-PEG-based nanoparticles grafted with GRGDS peptide: preparation and surface analysis by XPS. Biomacromolecules 8, 3977–3983.

Raymond, E., Hanauske, A., Faivre, S., Izbicka, E., Clark, G., Rowinsky, E.K., Von Hoff, D.D., 1997. Effects of prolonged versus short-term exposure paclitaxel (Taxol) on human tumor colony-forming units. Anticancer Drugs 8, 379–385.

Roch, A., Muller, R.N., Gillis, P., 1999. Theory of proton relaxation induced by superparamagnetic particles. J. Chem. Phys. 110, 5403–5411.

Roch, A., Gossuin, Y., Muller, R.N., Gillis, P., 2005. Superparamagnetic colloid suspensions: water magnetic relaxation and clustering. J. Magn. Magn. Mater. 293, 532–539.

Schiff, P.B., Fant, J., Horwitz, S.B., 1979. Promotion of microtubule assembly in vitro by taxol. Nature 277, 665–667.

Shieh, M.J., Hsu, C.Y., Huang, L.Y., Chen, H.Y., Huang, F.H., Lai, P.S., 2011. Reversal of doxorubicin-resistance by multifunctional nanoparticles in MCF-7/ADR cells. J. Control. Release 152, 418–425.

Singh, A., Dilnawaz, F., Mewar, S., Sharma, U., Jagannathan, N.R., Sahoo, S.K., 2011. Composite polymeric magnetic nanoparticles for co-delivery of hydrophobic and hydrophilic anticancer drugs and MRI imaging for cancer therapy. ACS Appl. Mater. Interfaces 3, 842–856.

Singla, A.K., Garg, A., Aggarwal, D., 2002. Paclitaxel and its formulations. Int. J. Pharm. 235, 179–192.

Talelli, M., Rijcken, C.J., Lammers, T., Seevinck, P.R., Storm, G., van Nostrum, C.F., Hennink, W.E., 2009. Superparamagnetic iron oxide nanoparticles encapsulated in biodegradable thermosensitive polymeric micelles: toward a targeted nanomedicine suitable for image-guided drug delivery. Langmuir 25, 2060–2067.

Weiss, R.B., Donehower, R.C., Wiernik, P.H., Ohnuma, T., Gralla, R.J., Trump, D.L., Baker Jr., J.R., Van Echo, D.A., Von Hoff, D.D., Leyland-Jones, B., 1990. Hypersensitivity reactions from taxol. J. Clin. Oncol. 8, 1263–1268.

Yang, X., Grailer, J.J., Rowland, I.J., Javadi, A., Hurley, S.A., Steeber, D.A., Gong, S., 2010. Multifunctional SPIO/DOX-loaded wormlike polymer vesicles for cancer therapy and MR imaging. Biomaterials 31, 9065–9073.

van Ewijk, G.A., Vroege, G.J., Philipse, A.P., 1999. Convenient preparation methods for magnetic colloids. J. Magn. Magn. Mater. 201, 31–33.